Correlation of Atmospheric Opacity Measurements by SCUBA and an Infrared Radiometer

Ian M. Chapman, David A. Naylor, Robin R. Phillips
Department of Physics, University of Lethbridge, 4401 University Dr., Lethbridge, Alberta, Canada, T1K 3M4

ABSTRACT

We present the results of a comparison of measured water vapour content above Mauna Kea obtained using SCUBA and an infrared radiometer at the JCMT. We show that for most weather conditions IRMA produces results that correlate well with the SCUBA measurements but that for nights with thick cirrus cover the IRMA results deviate from those obtained with SCUBA.

Key words: Radiative transfer, atmospheric effects.

1 INTRODUCTION

Ground based observatories operating at (sub)millimetre wavelengths are seriously hindered by the atmosphere, which absorbs, emits, and scatters electromagnetic radiation. Most of the opacity in this spectral region is due to the presence of several strongly-absorbing water vapour lines. Additional opacity arises from weaker transitions associated with molecular oxygen and ozone. To address this problem, (sub)millimetre observatories are built at dry, high altitude sites such as Mauna Kea, Hawaii (4100 m) and Chajnantor, Chile (5000 m). Locating a (sub)millimetre observatory at a high altitude site places it above much of the atmospheric water vapour, enabling astronomical observations in several semi-transparent spectral 'windows'. Even at these high altitude sites, however, there is still sufficient water vapour to affect observations. Furthermore, the highly polar nature of water molecules results in the non-uniform distribution of the species through the atmosphere. When this is coupled with bulk atmospheric motion above the telescope it results in rapid variations of the line-of-sight precipitable water vapour (pwv) abundance, giving rise to phase distortion of the wavefronts as they propagate through the atmosphere.

One method of correcting for wavefront phase distortion is to measure the amount of water vapour in the telescope beam. Traditionally, this has been derived through periodic skydip measurements, either with a dedicated tipping radiometer or with one of the primary telescope instruments. However, both methods have the disadvantage of yielding only an average measurement of pwv over the whole skydip rather than the desired value along the line-of-sight from the telescope to the source. Moreover, the former method uses an instrument that is offset from the main telescope beam, whereas the latter method requires interrupting observations to perform a skydip.

A more optimal solution is to have a device that looks along the telescope beam and directly determines the line-of-sight pwv column density without requiring skydips. For (sub)millimetre telescopes, one method has been to determine the amount water vapour from measurements of the 183 GHz water vapour line using a heterodyne receiver system. This involves measuring the intensity of three narrow bands offset by differing amounts from the line centre (which are hence sensitive to differing amounts of water vapour). This has the disadvantage of requiring a complex and difficult to maintain instrument.

We have developed an Infrared Radiometer for Millimetre Astronomy (IRMA) which employs a novel technique for measuring atmospheric water vapour content. The IRMA device is a simple infrared radiometer that observes a narrow spectral region around 20 μm (15 THz) which contains only rotational transitions of water vapour. The simplicity, and hence low cost and reliability of such a device, offers many advantages over the 183 GHz system. The ultimate goal for any water vapour monitor operating on a (sub)millimetre telescope is to provide measurements that enable water vapour induced atmospheric effects to be removed from the telescope science data. If IRMA is to be used in this capacity, the optical depth it measures at 20 μm must correlate directly with the optical depth at the operating wavelengths of the telescope (approximately 200 GHz - 1.2 THz or 1300 - 250 μm). This paper reports the results of a comparison of several months worth of IRMA data collected at the James Clerk Maxwell Telescope (JCMT) on Mauna Kea with several other sources of pwv available for this site.

2   ATMOSPHERIC OPACITY

The determination of the atmospheric opacity above Mauna Kea is critical for the calibration of astronomical data from the JCMT (Archibald et al. 2002). Precise measurements of the zenith sky opacity, τ, must be obtained frequently to ensure proper calibration of astronomical data. This is particularly critical for the JCMT's primary scientific instrument, the Submillimetre Common User Bolometer Array (SCUBA) (Holland et al. 1999). SCUBA uses one of its pixels in a DC biased mode to estimate the zenith sky opacity at the wavelength and azimuth of observation by performing periodic skydips. A skydip measures the emission of the atmosphere as a function of zenith angle. A radiative transfer model is then used to fit the data and determine the zenith sky opacity of the atmospheric windows used for the observation. SCUBA has been shown to provide an accurate estimate of τ provided that the weather conditions are stable and uniform across the sky (Archibald et al. 2002).

2.1   Radiative Transfer Model

In order to investigate the effect of atmospheric variations on the opacity of the windows observed by SCUBA, a radiative transfer model, known as the University of Lethbridge Transmission and Radiance Atmospheric Model (ULTRAM) (Chapman 2002), was developed using the Interactive Data Language (IDL®). IDL® was chosen for this project because of its many array handling routines which allow calculations of large data sets to be performed efficiently.

Like most radiative transfer models, ULTRAM is a *line-by-line, layer-by-layer* model. This description refers to the method used in the calculations: the contribution to opacity of each spectral line is computed separately and summed to give the overall opacity of an atmospheric layer as a function of wavenumber. This process is repeated for each of the layers descending from the top of the atmosphere to the ground.

Several radiative transfer models have presented in the literature. One which find frequent use is the Fast Atmospheric Signature Code (FASCODE) (Chetwynd et al. 1994). FASCODE has been developed to be a comprehensive radiative transfer model, with the ability to simulate nearly any desired observing geometry. The program has a number of built-in atmospheric models that describe the atmosphere in general geographic locations and seasons, such as the mid-latitude summer atmosphere.

While FASCODE has many strengths, it suffers from several limitations. The first is that the FASCODE atmospheric models all describe the atmosphere at general locations. To model a specific location a user has to carefully construct and format an atmospheric model to import into FASCODE. This is a complicated process that can easily lead to errors. Another limitation is that FASCODE is immense, with the main program alone consisting of over 71,000 lines of Fortran code. Because of its size, FASCODE is extremely difficult to maintain and modify for specific applications.

The limitations of FASCODE provided the impetus for the development of ULTRAM, whose goal was to simplify the generation of space-to-ground, location-specific atmo-
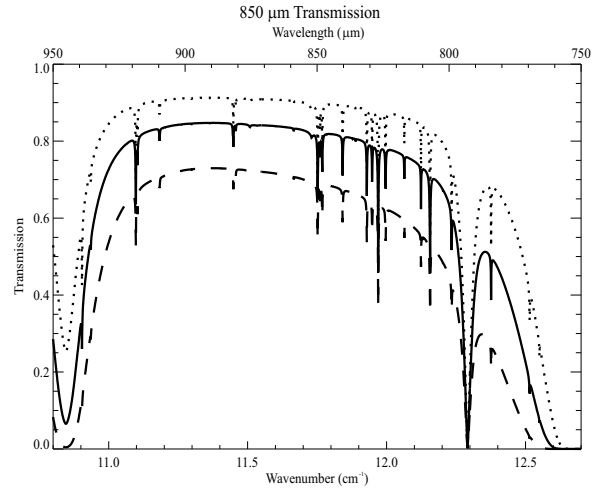

Figure 1. The transmission of the 850 μm window for the atmosphere above Mauna Kea with water vapour column abundances of 0.5 (dotted), 1.0 (solid), and 2.0 (dashed) mm pwv as modelled using ULTRAM.

spheric models. ULTRAM exploits the graphical user interface (GUI) and visualisation capabilities of IDL. Users can easily create and import atmospheric models through the use of a GUI or text files. A model of the atmosphere above Mauna Kea has been created using atmospheric parameters derived by averaging numerous radiosondes launched from nearby Hilo airport. This results in a more accurate spectrum for Mauna Kea than would be produced by the tropical atmosphere profile contained in FASCODE.

Although ULTRAM does not have the complex geometrical capabilities of FASCODE, it is a compact program designed to model atmospheric transmission for the astronomical community. Consisting of ∼1000 lines of a modern programming language, IDL®, ULTRAM is significantly more user-friendly and maintainable than other radiative transfer models. We have used ULTRAM extensively to generate the theoretical spectra presented in this paper.

A paper describing ULTRAM is currently in preparation. It is the authors' intention that ULTRAM be made freely available to the scientific community using the free IDL® Virtual Machine License once development of a graphical user interface is complete. Further information on ULTRAM can be obtained by contacting the authors.

2.2   Modelling the Atmosphere Above Mauna Kea

Under good observing conditions, the atmosphere above Mauna Kea has several (sub)millimetre windows, spectral regions where the atmosphere is semi-transparent. Two of these windows, centred on 850 μm and 450 μm and shown in Figs. 1 and 2 respectively, are those observed by SCUBA to determine atmospheric opacity. The main contributors to opacity in these spectral regions are water vapour, molecular oxygen, and ozone. The strongest transitions are those due to water vapour, which, since it exists mainly in the lower atmosphere, are dominated by pressure broadening resulting in a modified Voigt line shape (Clough et al. 1989). Ozone produces a manifold of weak, narrow lines. Since, in the tropics, the highest concentrations of ozone are found at an
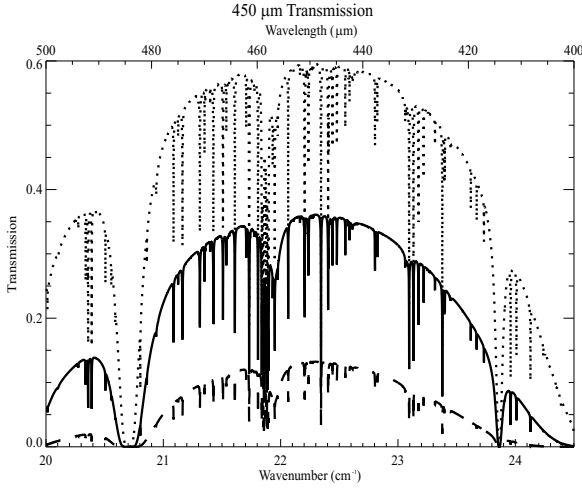
Figure 2. The transmission of the 450 μm window for the atmosphere above Mauna Kea with water vapour column abundances of 0.5 (dotted), 1.0 (solid), and 2.0 (dashed) mm pwv as modelled using ULTRAM.

Base Pressure	625 $mBar$
Base Temperature	273 K
Lapse Rate	-5.6 Kkm^{-1}
Scale Height	2 km
H_2O Column Amount	$3.346 * 10^{21}$ cm^{-2} (1 $mmpwv$)
CO_2 Column Amount	$4.395 * 10^{21}$ cm^{-2}
O_3 Column Amount	$7.497 * 10^{18}$ cm^{-2}
N_2O Column Amount	$3.964 * 10^{18}$ cm^{-2}
CO Column Amount	$1.189 * 10^{18}$ cm^{-2}
CH_4 Column Amount	$2.146 * 10^{19}$ cm^{-2}
O_2 Column Amount	$2.784 * 10^{24}$ cm^{-2}

Table 1. Input parameters for ULTRAM atmospheric model of the summit of Mauna Kea.

altitude of ~ 25 km, its line shape is dominated by thermal effects, resulting in a Doppler (Gaussian) profile.

The intensity of the radiation exiting the bottom of the atmosphere, I, in $Wm^{-2}sr^{-1}Hz^{-1}$ is related to the intensity of radiation entering the atmosphere from space, I_0, by the *radiative transfer equation*

$$I = I_0(e^{-\int_{z_0}^{l} k_\sigma n(z)dz}) + B(\sigma, T)(1 - e^{-\int_{z_0}^{l} k_\sigma n(z)dz}) \qquad (1)$$

where $n(z)$ is the number density of the absorbing species at altitude z, z_0 is the altitude of observation, l is the altitude of the top of the atmosphere, k_σ is the absorption coefficient of the atmosphere at wavenumber, σ, and $B(\sigma, T)$ is the Planck blackbody function at σ, and temperature, T. Since τ is defined as $\int_{z_0}^{l} k_\sigma n(z)dz$, Eq. 1 can be written as

$$I = I_0(e^{-\tau}) + B(\sigma, T)(1 - e^{-\tau}) \qquad (2)$$

In practice, Eq. 2 is modified to include radiative effects due to emission from components in the optical train of the telescope, J_{tel}. For example, for the JCMT this would include emission from the membrane and the warm telescope optics. The modified radiative transfer equation can be written as

$$I = I_0(e^{-\tau}) + B(\sigma, T)(1 - e^{-\tau}) + J_{tel} \qquad (3)$$

The first term in Eq. 3 describes the absorption of radiation that originates from space. SCUBA skydips assume that no bright astronomical sources are sampled, so the only radiation from space is due to the cosmic microwave background (CMB). Emissions from the atmosphere sufficiently dominate the CMB in these wavelengths, so the absorption term can be neglected in Eq. 3, leaving

$$I = B(\sigma, T)(1 - e^{-\tau}) + J_{tel} \qquad (4)$$

Under the assumption of a plane-parallel atmosphere and integrating over the spectral band, Eq. 4 can be expressed in terms of the zenith angle, θ, or equivalently airmass, A, defined as $sec\theta$. Eq. 4 becomes

$$I = \int_{band} (B(\sigma, T)(1 - e^{-\tau}) + J_{tel})d\sigma \qquad (5)$$

Data from the measured skydips are fitted to this equation to produce τ-values.

While SCUBA determines τ by fitting an atmospheric model to the skydips it obtains, ULTRAM has been used to determine theoretical τ-values through direct calculations. An opacity cube has been produced by using ULTRAM to model the atmosphere above Mauna Kea for the wavenumber range of 5 to 50 cm^{-1} (2000 to 200 μm) as a function of water vapour column abundance (0 to 2 mm pwv in steps of 0.1 mm pwv). Base conditions for the atmospheric model were determined by averaging data from radiosondes which are launched twice daily (0:00 and 12:00 UT) from Hilo airport, approximately 40 km from Mauna Kea. Data from 80 radiosondes launched in the evenings (12:00 UT) from June to October of 2000, downloaded from http://weather.uwyo.edu/upperair/sounding.html, were averaged and the results are shown in Table 1. Table 1 also shows the column amounts of the molecules used in the Mauna Kea simulations which were determined using molecular mixing ratios taken from the tropical atmosphere profile in FASCODE3 (Chetwynd et al. 1994). The temperature and pressure profiles for the lower atmosphere (4.092 to 12 km) were determined from the base conditions in Table 1, while those in the upper atmosphere (above 12 km) were taken from the FASCODE3 tropical atmosphere profile. The modelled Mauna Kea pressure-temperature curve is shown in Fig. 3. The 850 and 450 μm spectral bands are defined by the filter profiles of SCUBA (Naylor & Holland 2001).

A theoretical τ-value has been determined for each water vapour column abundance in the data cube by averaging the modelled opacity over each of the 850 and 450 μm spectral bands. Eq. 5 shows that the value of τ varies linearly with airmass (or equivalently, water vapour column abundance), so linear regression was used to determine a relation between the two quantities. For the 850 μm window, the column abundance of water vapour can be expressed as a function of opacity

$$pwv = 4.10\tau_{SCUBA850} - 0.36 \qquad (6)$$

The corresponding relation for the 450 μm window is

$$pwv = 0.83\tau_{SCUBA450} - 0.04 \qquad (7)$$

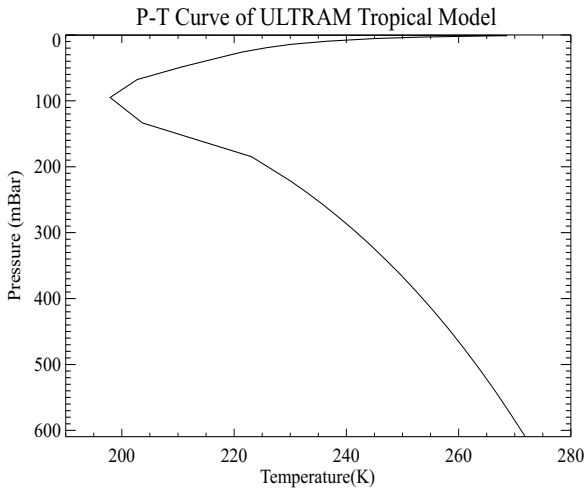Relations between $\tau_{SCUBA850}$ and τ_{CSO225}, and

Figure 3. The pressure-temperature curve from the ULTRAM atmospheric model for Mauna Kea.

$\tau_{SCUBA450}$ and τ_{CSO225} have been experimentally determined (Archibald et al. 2002) to be

$$\tau_{SCUBA850} = 4.02\tau_{CSO225} - 0.004 \tag{8}$$

and

$$\tau_{SCUBA450} = 26.2\tau_{CSO225} - 0.37 \tag{9}$$

respectively.

A relation between water vapour column amount and τ_{CSO225} (Davis et al. 1997) has been determined to be

$$pwv = 20\tau_{CSO225} - 0.32 \tag{10}$$

Combining Eq. 10 with Eqs. 8 and 9 and rearranging for pwv yields

$$pwv = 5.0\tau_{SCUBA850} - 0.30 \tag{11}$$

and

$$pwv = 0.76\tau_{SCUBA450} - 0.04 \tag{12}$$

We believe that the theoretical relations in Eqs. 6 and 7 are more accurate than the relations we derived from the SCUBA/CSO τ relations (Archibald et al. 2002) since the data cube produced by ULTRAM was based on radiosonde data from the atmosphere above Mauna Kea. By comparison, Eqs. 11 and 12 are derived from Eqs. 8 and 9 respectively, which make use of the US Standard Atmosphere 1976 (Hazell 1991) which is not representative of the atmosphere above Mauna Kea.

3   IRMA CONCEPT

Measurements of atmospheric opacity above Mauna Kea in the 20 μm atmospheric window using a high resolution infrared Fourier transform spectrometer have shown that over a large part of this region, the atmospheric absorption, and hence emission, is dominated by pure rotational transitions of water vapour (Naylor et al. 1984). Detailed modelling shows that it is possible to select a continuous region containing several hundred water vapour lines, the vast majority of which are unsaturated for column abundances of $\leqslant 1$ mm

Total Number of IRMA Skydips	1893
Number Time-Matched With SCUBA	613
Number Rejected For Poor Quality	80
Number Used In Comparison With SCUBA	533
Number Used In Comparison With CSO	1278

Table 2. A summary of the IRMA skydips collected over the period from December 2000 to March 2001.

pwv above Mauna Kea. At lower altitude sites the lines in this spectral region become saturated and thus the technique becomes less sensitive.

An infrared approach to water vapour measurement is attractive for several reasons. Firstly, since the wavelength of 20 μm lies near the peak of the Planck curve for typical atmospheric temperatures, the spectral radiance from atmospheric water vapour at infrared wavelengths is ~ 3 orders of magnitude greater than at radio frequencies. Secondly, the infrared radiometer uses a spectral bandwidth ~ 3 orders of magnitude greater than the radio frequency technique. The resulting increase in flux can be traded in terms of more sensitive measurements, faster operation, smaller instrument size, or some combination thereof. Thirdly, infrared photoconductive detectors offer high operating speeds, stability, and simple electronics. Finally, being a passive device (specifically, not containing a local oscillator), an infrared radiometer can be placed in close proximity to sensitive radio frequency instrumentation without risk of interference.

A prototype infrared radiometer for the measurement of atmospheric water vapour (IRMA I) was developed and tested at the JCMT in December 1999 (Smith et al. 2001). The radiometer consisted of a liquid nitrogen cooled Mercury-Cadmium-Telluride (MCT) photoconductive detector that alternately viewed the atmosphere, and ambient and liquid nitrogen blackbody references. This was accomplished by means of a stationary parabolic mirror and a scanning plane mirror. The scanning mirror provided a range of observable zenith angles from 0 to 70.38 degrees in steps of 0.18 degrees, corresponding to an airmass range from 1 to 3. The optical input to the detector was chopped at 200 Hz by a reflective chopper blade so that the detector was alternately presented with views of the atmosphere (or the blackbodies) and a reflected view of its own cold environment. The modulated detector signal was amplified, synchronously detected by means of a lock-in amplifier, digitized by a 12-bit analog-to-digital converter (ADC) and the resulting data was logged to a file.

The radiometer was primarily operated in *continuous scan* mode in which the atmospheric emission was measured as a function of airmass, these data being referred to as *skydips* (a skydip of 1 to 3 airmass taking ~ 30 s). IRMA can also be operated in *stare mode*, pointing along the line-of-sight of astronomical observations. In this mode, IRMA makes observations at a rate of 10 Hz, periodically performing skydips (~ 1 per hour) for calibration.

Analysis of the IRMA I skydips showed that the infrared technique held much promise for the challenging requirements of phase correction of the next generation of (sub)millimetre interferometers. Key elements of the prototype radiometer were subsequently improved, and include: a more sensitive MCT photoconductive detector, a resonant
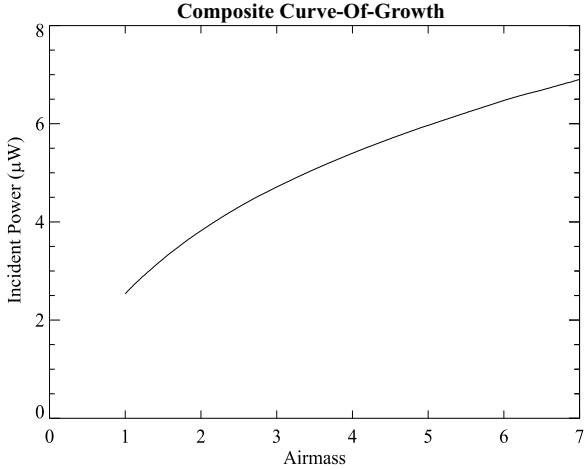
Figure 4. The mean, composite curve-of-growth determined from individual IRMA skydips which forms the basis for establishing τ_{IRMA} in Eq. 14 for comparison with $\tau_{SCUBA850}$, $\tau_{SCUBA450}$, and τ_{CSO225}. In this figure, the incident power at an airmass of 1 corresponds to a water vapour column abundance of 0.5 mm pwv (Chapman 2002).

grid long pass filter (Lee et al. 1996) (this technology is well established at submillimetre and far-infrared wavelengths but has only recently been extended to shorter wavelengths), a custom lock-in amplifier, and a high-resolution (24-bit) $\Delta\Sigma$ analog-to-digital converter, which is synchronously triggered by a notch on the reflecting chopper wheel.

Finally, the IRMA software was modified to allow for remote operation. This paper presents results obtained with IRMA operating on the apron of the JCMT between December 2000 and March 2001.

4 ANALYSIS METHOD

4.1 Curve-of-Growth

Between December 2000 and March 2001, IRMA was set up to collect a series of skydips simultaneously with SCUBA skydips. A total of 1893 IRMA skydips were obtained during this period. Due to IRMA's location outside of the JCMT membrane, it did not share exactly the same azimuthal angle as the telescope due to small offsets between the carousel and telescope. However, the alignment was sufficiently close that we expected the IRMA and SCUBA skydips would be correlated. The number of IRMA skydips for which corresponding SCUBA skydips exist is 613. The data were then filtered based on the quality of the skydips. Low quality skydips, caused by factors such as cryogen depletion or scanning past atmospheric cloud banks, were identified by either high or low voltages, or by poor fit with an exponential curve (i.e.. wavy skydips). These flagged skydips were removed from the data set, leaving 533, or $\sim$ 87 per cent, of the time-matched subset (see Table. 2).

As a part of the skydip cycle, IRMA obtained several calibration measurements of hot and cold loads, allowing a determination of the instrumental responsivity, R_{inst} (VW^{-1}), which relates the incident power on the radiometer, Φ (W), to the voltage measured, V, by
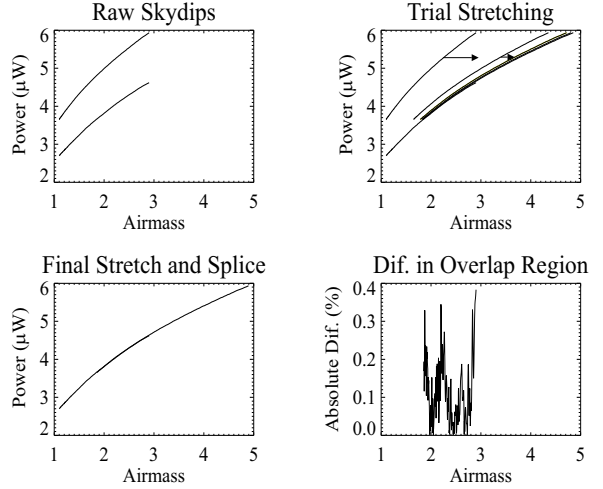

Figure 5. Sample output from the stretch-and-splice routine used in the analysis of IRMA data. The upper skydip in the top left panel was collected during a time of higher atmospheric water vapour content than the lower skydip. In the top right panel the fitting routine guesses several stretch factors before finding the optimal value, which is shown in the bottom left panel. The bottom right panel shows the absolute difference between the skydips in the final overlapping area.

$$\Phi = \frac{V}{R_{inst}} \qquad (13)$$

Using this equation, the skydips were calibrated to give incident power as a function of airmass.

Once calibrated, the data can be used to generate a *curve-of-growth* (Houghton 1986), as in Fig. 4, which shows the spectrally integrated emission of an absorbing species as the abundance of the species is varied. In the case of the atmosphere, the abundance of water vapour is varied by the process of performing a skydip; observing the sky at increasing zenith angles, or equivalently, airmass. To simplify the analysis, it is assumed that the vertical pressure and temperature profiles and water vapour scale height do not vary significantly from day to day. Analysis of 80 pressure-temperature curves from radiosondes, launched from nearby Hilo airport, supports this assumption.

Under these assumptions it is possible to construct a curve-of-growth by rescaling, or *stretching*, the horizontal axes of the individual skydips to reflect the water vapour amount at the times of observation. Fig. 5 shows 2 IRMA skydips in the upper left panel. The higher skydip was collected at a time of higher water vapour content than the lower. Stretching is accomplished by using a fitting routine to find a stretch factor, F, where the difference of the overlapping region between the top and the bottom skydips is minimized. This step is shown in the upper right panel of Fig. 5. The top skydip is stretched to fit the lower skydip by the fitting program until an optimal stretch factor is found. The upper skydip is in its optimal position in the bottom left panel of the figure, with the absolute per cent difference between the overlapping sections of the skydips shown in the bottom right panel. The upper skydip is then *spliced* to the lower by averaging the overlapping regions of the 2 skydips. This process is termed *stretch-and-splice*.

Using the stretch-and-splice method a *basis curve-of-growth* is constructed from 5 IRMA skydips chosen to cover
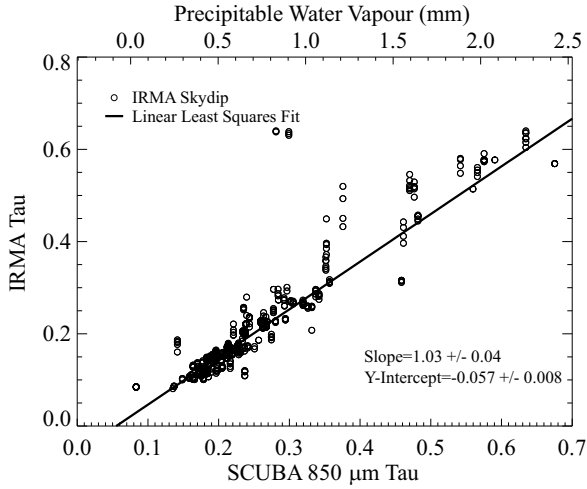
Figure 6. Comparison of IRMA and SCUBA 850 μm atmospheric opacity measurements.

Figure 7. Comparison of IRMA and SCUBA 450 μm atmospheric opacity measurements.

the entire vertical range of the dataset. A *mean, composite curve-of-growth* is generated from all of the skydips by stretch-and-splicing each to the basis curve-of-growth. A base opacity for the IRMA 20 μm spectral region, or τ_{IRMA}, is determined by fitting the mean, composite curve-of-growth to an exponential function and taking the value of the exponent as τ^*_{IRMA}. The IRMA skydips are then fitted to the mean, composite curve-of-growth using the stretch-and-splice method, and the stretch factors, F, from the fitting routine are used to determine a τ_{IRMA} for the individual skydips using the simple relation

$$\tau_{IRMA} = \tau^*_{IRMA} \times F \qquad (14)$$

These resulting IRMA opacities can then be compared to the corresponding time-matched SCUBA opacities.

5   RESULTS

5.1   SCUBA 850 μm

Fig. 6 shows τ_{IRMA} plotted against $\tau_{SCUBA850}$. In this figure each circle represents the τ value calculated for a single IRMA skydip. Circles appear in vertical groups because several IRMA skydips can be performed during a single SCUBA skydip. The appearance of columnar grouping in the data indicates that the atmospheric water vapour content is changing appreciably during the time that SCUBA performs a skydip ($\sim$7 minutes). The linear least squares fit to the data is also shown. Most of the data points are tightly clustered about the line, indicating a high degree of correlation between the measurements, as expected. The correlation coefficient for this data is $r^2 = 0.924$. The slope of the line shows that the 850 μm spectral region saturates slightly faster than the infrared region observed by IRMA. The non-zero intercept of the line indicates that water vapour is not the only species responsible for atmospheric opacity in the 850 μm band. Atmospheric modelling (see Fig. 1) shows this nonzero intercept is to be expected since the 850 μm region contains numerous ozone and oxygen lines which provide an additional source of opacity not present at 20 μm. The top scale in Fig. 6, calculated from Eq. 6, shows that the x-intercept
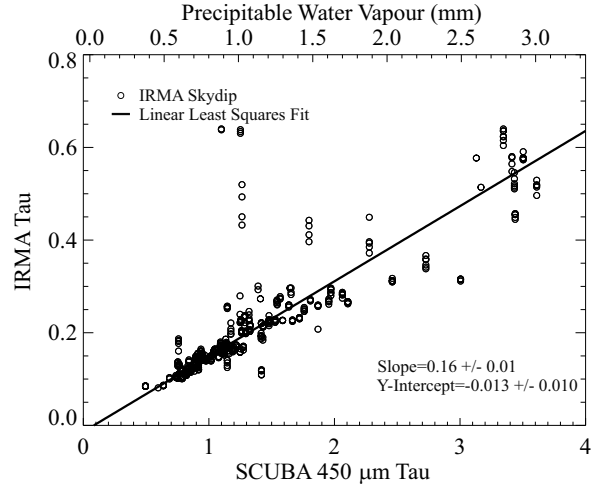
of the least squares fit falls close to 0 mm pwv, indicating that IRMA is only sensitive to atmospheric water vapour.

5.2   SCUBA 450 μm

Fig. 7 shows τ_{IRMA} plotted against $\tau_{SCUBA450}$. As in Fig. 6, each circle represents the τ value calculated for an IRMA skydip. Circles again appear in vertical groups because the atmospheric water vapour content changes appreciably during a single SCUBA skydip. The linear least squares fit to the data is shown, and again a high degree of correlation (correlation coefficient, $r^2 = 0.867$) is indicated by the tight clustering of circles about the line. The slope of the line shows that the 450 μm spectral region saturates much faster than the infrared region observed by IRMA. The small, non-zero intercept of the line indicates that water vapour is the main species responsible for atmospheric opacity in the 450 μm region with a small amount of opacity due to numerous ozone lines (see Fig. 2). However, this additional opacity due to the stratospheric ozone lines in the 450 μm region is less significant because the opacity due to tropospheric water vapour is much higher in this region. The top scale in Fig. 7, calculated from Eq. 7, again shows that IRMA only measures opacity due to atmospheric water vapour.

5.3   CSO 225 GHz Tau

The Caltech Submillimetre Observatory (CSO) (Phillips 1990) operates a 225 GHz skydipper that for many years has been the primary source of opacity measurements for the (sub)millimetre telescopes on Mauna Kea. It was operating for most of the IRMA run and returns an opacity value every 10 minutes, thereby yielding a large dataset against which the IRMA skydips can be compared. However, the CSO skydips have a reputation of being unreliable around sunrise and sunset and can also have large errors in weather that is changing rapidly (since the skydip is an average of the whole sky in the direction that the dipper is pointing). To minimise these problems, the JCMT produces a 'CSO fits' archive (online at   www.jach.hawaii.edu/JAClocal/JCMT/jcmt_tau.html)
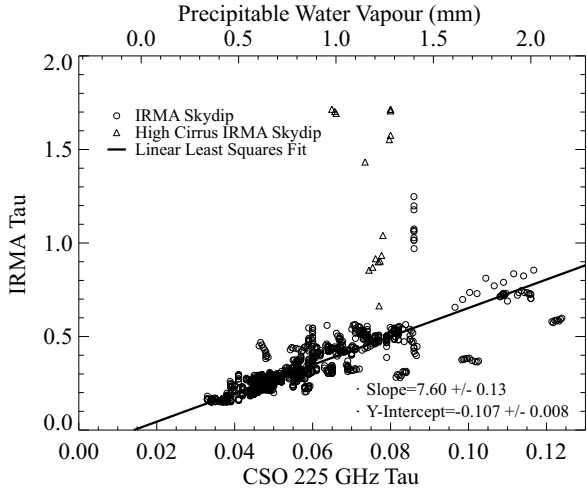
Figure 8. Comparison of IRMA and CSO 225 GHz atmospheric opacity measurements.

Comparison Instrument	Correlation Coefficient
SCUBA 850 μm	0.924
SCUBA 450 μm	0.867
CSO 225 GHz (cirrus included)	0.716
CSO 225 GHz (cirrus excluded)	0.844

Table 3. A summary of the correlation coefficients for the τ_{IRMA} comparisons.

which is a subset of all CSO skydips that have been filtered to include only those points that have a nearby SCUBA skydip that returned a similar value. A smooth polynomial is then fitted to these data points which can then be used to give a CSO value for any time for which a fit is available. Fig. 8 shows all of the continuous IRMA skydips (1278) for which there was an available CSO fit. This produces a considerably better fit than the equivalent figure with the unfiltered CSO data points. The correlation coefficient for this data is $r^2 = 0.716$. Eq. 10 is used to produce the top scale in Fig. 8, which relates τ_{CSO225} to atmospheric water vapour content.

One of the main concerns with the IRMA concept is that the opacity in the 20 μm wavelength range is affected by the presence of cirrus clouds which have little impact at wavelengths of 1 mm. Unfortunately during the IRMA campaign at the JCMT we did not have a method in place for tracking the amount of cirrus on any given night. We are not aware of any automated systems (e.g.: all sky cameras) that were operating on Mauna Kea in 2000. However, the UKIRT telescope operators keep a written log of the weather conditions with an estimate of the cirrus cover on a scale of 1 to 8. We obtained this log and checked for nights during the IRMA campaign where the estimate was $\frac{7}{8}$ or $\frac{8}{8}$ of cirrus cover. For the 40 day IRMA campaign there was only one night where this level of cirrus cover was recorded; the corresponding points are plotted as triangles on Fig. 8. The log notes than on this night the cirrus was sufficiently thick that UKIRT was unable to operate.

It can be clearly seen that in the extreme case (that occurred once in the 40 day period) IRMA does generate incorrect readings. The remaining vertical column of points and the three groupings of points well below the best fit line both come from the last couple of days of operation in March just before the instrument failed – possibly implying some other problem with these data. However, the rest of the data, taken over the time period from mid December to early February, is a remarkably good fit especially considering that the CSO τ meter is pointing in a fixed azimuth position which is generally different than the JCMT. The correlation coefficient of the data in Fig. 8 is $r^2 = 0.844$ if the cirrus

is not included, nearly as high as the correlation of τ_{IRMA} with $\tau_{SCUBA850}$.

Further analysis to determine a relationship between the number of 'eighths' entered in the UKIRT log and the distance from the line of best fit for points on a given night showed no detectable trend.

We draw two conclusions from this (data limited) analysis of cirrus effects. 1) Small amounts of cirrus as is fairly common on Mauna Kea have no detectable effect on the IRMA data and 2) Nights where the cirrus is thick enough to be problematic at infrared wavelengths are uncommon.

Future IRMA campaigns will attempt to address this issue further. We note that a potential solution would be to add a second infrared detector channel, specifically tuned to measure cirrus emission, which could then be removed in post-processing.

6 CONCLUSIONS

Measurements of the column abundance of atmospheric water vapour above Mauna Kea obtained with an infrared radiometer show a high degree of correlation with other measures of water vapour available on the summit of Mauna Kea. Correlation coefficients for each of the SCUBA and CSO comparisons are shown in Table 3.

The lines of best fit through the comparison data shows that on nights that IRMA is unaffected by cirrus clouds, it measures exclusively water vapour emission while some of the opacity in the bands observed by SCUBA is due to other species. Relations between τ_{IRMA} and opacity measurements from the comparison instruments are given in Table 4. This is evidenced by the non-zero x-intercepts of the linear least squares fits in the figures that correspond to water vapour column abundances of 0 mm pwv. Atmospheric modelling shows that this additional opacity is due to molecular oxygen and ozone.

IRMA measurements of atmospheric opacity also show a correlation with corresponding measurements made by the 225 GHz skydipper (see Fig. 8). Although these data sets are less well correlated, this is not unexpected because the CSO τ-meter is located on a different part of Mauna Kea and operates at a fixed azimuth. Even so, the linear least squares fit to the data again intersects the x-axis at a τ-value corresponding to a water vapour column abundance of 0 mm pwv, indicating that IRMA is sensitive to water vapour alone.

A third, improved version of IRMA will soon be completed and tested in June 2004 at Mauna Kea. These new IRMA devices are more self contained than the previous versions and are designed to operate for long periods of time requiring no maintenance. The goal of the site tests is to

Comparison Instrument	Tau Relation
SCUBA 850 μm	$\tau_{IRMA} = 1.03\tau_{SCUBA850} - 0.057$
SCUBA 450 μm	$\tau_{IRMA} = 0.16\tau_{SCUBA450} - 0.013$
CSO 225 GHz	$\tau_{IRMA} = 7.60\tau_{CSO225} - 0.107$

Table 4. A summary of the relations between τ_{IRMA} and opacity measurements from the comparison instruments (SCUBA and CSO).

prove that IRMA is a powerful water vapour detector for use in phase-delay compensation for radio telescope arrays.

7   ACKNOWLEDGEMENTS

REFERENCES

Archibald E. N., Jenness T., Holland W. S., Coulson I. M., Jessop N. E., Stevens J. A., Robson E. I., Tilanus R. P. J., Duncan W. D., Lightfoot J. F., 2002, MNRAS, 336, 1

Chapman I. M., 2002, Master's thesis, University of Lethbridge, Alberta, Canada

Chetwynd J. H., Wang J., Anderson G. P., 1994, in Proc. SPIE Vol. 2266, Optical Spectroscopic Techniques and Instrumentation for Atmospheric and Space Research, Jinxue Wang; Paul B. Hays; Eds. Fast Atmospheric Signature CODE (FASCODE): an update and applications in atmospheric remote sensing. pp 613–623

Clough S. A., Kneizys F. X., Davies R., 1989, Atmospheric Research, 23

Davis G. R., Naylor D. A., Griffin M. J., Clark T. A., Holland W. S., 1997, Icarus, 130

Hazell A. S., 1991, PhD thesis, University of London

Holland W. S., Robson E. I., Gear W. K., Cunningham C. R., Lightfoot J. F., Jenness T., Ivison R. J., Stevens J. A., Ade P. A. R., Griffin M. J., Duncan W. D., Murphy J. A., Naylor D. A., 1999, MNRAS, 303, 659

Houghton J. T., 1986, The Physics of Atmospheres. Cambridge University Press

Lee C., Ade P. A. R., Haynes C. V., 1996, in Proceedings of the 30th ESLAB Symposium Self Supporting Filters for Compact Focal Plane Designs

Naylor D. A., Boreiko R. T., Clark T. A., Emery R. J., Fitton B., Kessler M. F., 1984, PASP, 96, 167

Naylor D. A., Holland W. S., 2001, Technical report, Measuring the SCUBA wideband filters using the University of Lethbridge FTS.. JCMT

Phillips T. G., 1990, in From Ground-Based to Space-Borne Sub-mm Astronomy The Caltech Submillimeter Observatory

Smith G. J., Naylor D. A., Feldman P. A., 2001, Int. J. of Inf. and Mm. Waves, 22, 661